Infrared spectroscopy study of the nodal-line semimetal candidate ZrSiTe under pressure: Hints for pressure-induced phase transitions

J. Ebad-Allah,[1,2] M. Krottenmüller,[1] J. Hu,[3] Y. L. Zhu,[4,5] Z. Q. Mao,[4,5] and C. A. Kuntscher[1,*]

[1]*Experimentalphysik II, Augsburg University, 86159 Augsburg, Germany*

[2]*Department of Physics, Tanta University, 31527 Tanta, Egypt*

[3]*Department of Physics, University of Arkansas, Fayetteville, Arkansas 72701, USA*

[4]*Department of Physics, Pennsylvania State University, University Park, Pennsylvania 16803, USA*

[5]*Department of Physics and Engineering Physics, Tulane University, New Orleans, Louisiana 70118, USA*

(Received 3 May 2019; published 19 June 2019)

We studied the effect of external pressure on the optical response of the nodal-line semimetal candidate ZrSiTe by reflectivity measurements. At pressures of a few GPa, the reflectivity, optical conductivity, and loss function are strongly affected in the whole measured frequency range (200–16 500 cm^{-1}), indicating drastic changes in the electronic band structure. The pressure-induced shift of the electronic bands affects both the intraband and interband transitions. We find anomalies in the pressure dependence of several optical parameters at the pressures $P_{c1} \approx 4.1$ GPa and $P_{c2} \approx 6.5$ GPa, suggesting the occurrence of two phase transitions of either structural or electronic type.

DOI: 10.1103/PhysRevB.99.245133

Topological semimetal materials such as Dirac, Weyl, and nodal line semimetals are of a great current interest due to their exceptional physical properties, including high bulk carrier mobility and large magnetoresistance [1–7]. Over the last few years, nodal-line semimetals (NLSMs) attracted increasing attention due to their multiple band crossings along a line in momentum space, in contrast to Dirac and Weyl semimetals, where the bands are touching at discrete k points. ZrSiS and its isostructural compounds ZrXY (X = Si, Ge, Sn and Y = O, S, Se, Te) are NLSM candidates, where electronic band-structure calculations showed multiple linear band crossings at various energies [8–10]. ZrXY compounds have a PbFCl-type structure (tetragonal P4/nmm space group with nonsymmorphic symmetry), where the Zr atoms are coordinated by four carbon group atoms X and four chalcogen atoms Y [11]. The Zr, X, and Y atoms are arranged in square nets parallel to the ab plane. Accordingly, the crystal structure of the ZrXY compound is layered, consisting of slabs with five square nets and the stacking sequence [Y-Zr-X-Zr-Y].

Several studies reported that the unique electronic properties of ZrXY compounds are mainly determined by the carbon group X square sublattice and that the structural dimensionality can be tuned by isoelectronic substitution of either chalcogen element Y or the carbon group element X [9,11–13]. For example, tuning the chalcogen atom from S to Te increases the ionic radius and the ratio of lattice parameters c/a, concomitant with the decrease of the interlayer bonding [8,14,15]. Accordingly, ZrSiTe is expected to be more two-dimensional (2D) as compared to ZrSiS regarding its electronic properties [11]. Indeed, de Haas–van Alphen quantum measurements revealed a 2D character of the Fermi surface (FS), in addition to a 3D component, in contrast to ZrSiS (as well as ZrSiSe) with a 3D-like FS [16].

Within the ZrXY compound family, ZrSiS is the most studied one. ZrSiS has an almost ideal nodal-line electronic band structure with a diamond-rod-shaped FS, although spin-orbit coupling opens up a small energy gap (∼0.02 eV) at the Dirac nodes [9,15,17]. Additional Dirac-like band crossings, which are protected by nonsymmorphic symmetry against gapping (called nonsymmorphic band crossings in the following), are located several hundred meV above and below the Fermi energy at the X and R point of the Brillouin zone. These nonsymmorphic band crossings were suggested to host 2D Dirac fermions with unusual electronic properties [9,18]. Recent density functional theory calculations [15] showed that such band crossings are also present in other ZrXY compounds, and that their energy position depends on the c/a ratio, i.e., the dimensionality of the system: For compounds with c/a ratios between 2.2 and 2.3, as in ZrSiS, the nonsymmorphic band crossings are located ∼0.6 eV above and below the Fermi energy (E_F), with an energy separation $\Delta E_{bc} \sim 1.2$ eV. For ZrSiTe with a much larger c/a ratio (≈2.57) and corresponding enhanced two dimensionality, these band crossings are shifted towards E_F with $\Delta E_{bc} \sim 0.4$ eV, thus suggesting ZrSiTe to be a real material that exhibits nonsymmorphic band crossings close to E_F [15].

The near-E_F band structure of ZrSiTe thus contains the linear crossing bands of the nodal line, although in comparison to ZrSiS slightly shifted in energy and more gapped due to the larger spin-orbit coupling. Additionally, there are nonsymmorphic band crossings close to E_F in the vicinity of the X-R line, which distort the nodal-line structure along the X-R line, and the Fermi level is pushed away from the nodal line in the rest of the Brillouin zone [19]. It was furthermore shown that ZrSiTe has a diamond-shaped FS, similar to ZrSiS,

*christine.kuntscher@physik.uni-augsburg.de

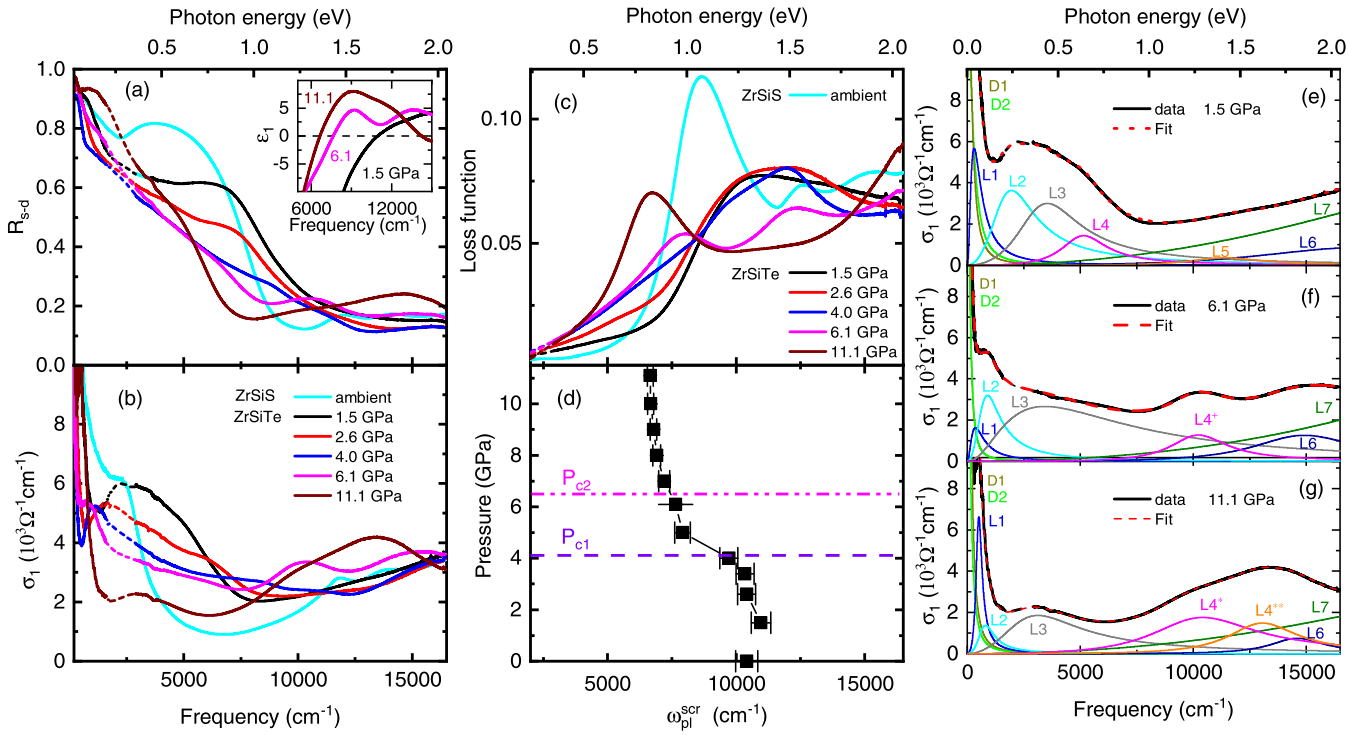

FIG. 1. Room-temperature optical response functions of ZrSiTe for selected pressures compared to ambient-pressure ZrSiS: (a) reflectivity R_{s-d} at the sample-diamond interface, (b) real part of the optical conductivity σ_1, (c) loss function $-\mathrm{Im}(1/\hat{\epsilon})$. The part of the optical response functions, which is affected by the multiphonon absorption in the diamond, is indicated by a dashed line. Inset of (a): Real part of the dielectric function $\epsilon_1(\omega)$ of ZrSiTe at 1.5, 6.1, and 11.1 GPa. (d) Screened plasma frequency ω_{pl}^{scr} of ZrSiTe as a function of pressure, determined from the zero-crossing energy of $\epsilon_1(\omega)$. The pressure P_{c1} (P_{c2}) is marked by a dashed (dash-dotted) line. (e)–(g) Optical conductivity spectra of ZrSiTe at 1.5, 6.1, and 11.1 GPa, respectively, together with the total fit and the various Drude (D) and Lorentz (L) contributions.

but with extra small pockets, most probably of a holelike nature [20].

The application of external pressure is a superior way for tuning the dimensionality of a system, as compared to isoelectronic substitution (chemical pressure). In ZrSiS hydrostatic pressure has the strongest effect on the c lattice parameter, which is perpendicular to the square lattice plane, resulting in a pressure-induced decrease of the c/a ratio [21]. In analogy, applying hydrostatic pressure on ZrSiTe, which is more 2D as compared to ZrSiS, a dimensionality change from 2D towards more 3D is expected, concomitant with the decrease of the c/a ratio. According to Topp *et al.* [15], the energy separation ΔE_{bc} of the nonsymmorphic band crossings at the X point of the Brillouin zone increases with decreasing c/a ratio. Thus, ZrSiTe is expected to have an increased ΔE_{bc} under pressure.

Indeed, in our infrared spectroscopy study of ZrSiTe under external pressure, we find indications of such changes in the electronic band structure at low pressures. The optical response functions are strongly affected by the pressure application. In particular, we observe anomalies in several optical parameters, signaling the occurrence of two pressure-induced phase transitions.

The optical response functions of ZrSiTe at the lowest studied pressure (1.5 GPa), depicted in Fig. 1 [22], are in good agreement with the ambient-pressure results reported recently [19]. We show here the reflectivity R_{s-d} measured at the sample-diamond interface, the real part of the optical conductivity σ_1, and the loss function, defined as $-\mathrm{Im}(1/\hat{\epsilon})$ where $\hat{\epsilon}$ is the complex dielectric function (see the Supplemental Material for details on experiment and analysis of data [22]). The reflectivity R_{s-d} is high at low frequencies, indicating the metallic state, but drops with increasing frequency and saturates above 2500 cm^{-1}, forming a plateau in the range 2500–7000 cm^{-1} [see Fig. 1(a)]. The further rapid decrease of reflectivity above $\approx$7000 cm^{-1} marks the onset of the plasma edge, which is followed by a featureless, low reflectivity above $\approx$12 000 cm^{-1}. The plasma edge in ZrSiTe at 1.5 GPa is rather broad and not well defined because of the plateau. This is also revealed by the loss function, which does not contain a clear plasmon mode [Fig. 1(c)]. In contrast, for ZrSiS at ambient pressure the reflectivity spectrum shows a rather sharp plasma edge [Fig. 1(a)], and the corresponding loss function [Fig. 1(c)] contains a well-defined peak at the screened plasma frequency $\omega_{pl}^{scr} \approx 8650$ cm^{-1}, which corresponds to the intraband plasmon. Alternatively, ω_{pl}^{scr} can be determined from the zero crossing of the real part of the dielectric function, $\epsilon_1(\omega)$ [23]. According to the zero crossing of $\epsilon_1(\omega)$ [inset of Fig. 1(a)], we obtain $\omega_{pl}^{scr} = 11\,000$ cm^{-1} for ZrSiTe at 1.5 GPa.

The optical conductivity σ_1 for ZrSiTe at 1.5 GPa contains Drude contributions at low frequencies related to the itinerant charge carriers and a broad absorption band centered at around 3200 cm^{-1} due to excitations between electronic bands close to E_F [see Fig. 1(b)]. Above 8000 cm^{-1} the optical conductivity monotonically increases with increasing frequency which signals the onset of higher-energy interband transitions.

The contributions to the optical conductivity at 1.5 GPa, as obtained by Drude-Lorentz fitting, are depicted in Fig. 1(e) (see also the Supplemental Material [22]): The low-energy optical conductivity is described by two Drude terms $D1$ and $D2$ and one sharp Lorentzian term $L1$. The two Drude contributions in ZrSiTe are consistent with the presence of electron- and hole-type itinerant charge carriers, with the prevalence of the latter according to magnetotransport measurements [20]. From the spectral weight of the Drude contributions we obtain the plasma frequency $\omega_{pl} = 20.000 \pm 1400$ cm^{-1} according to the sum rule $\omega_{pl}^2/8 = \int_0^\infty [\sigma_{1,D1}(\omega) + \sigma_{1,D2}(\omega)]d\omega$ [23,24]. The plasma frequency ω_{pl} is related to the screened plasma frequency ω_{pl}^{scr} according to $\omega_{pl}^{scr} = \omega_{pl}/\sqrt{\epsilon_\infty}$, where ϵ_∞ is the high-frequency value of $\epsilon_1(\omega)$. Hence, one obtains $\epsilon_\infty \approx 3.3$, in good agreement with $\epsilon_1(\omega)$ depicted in the inset of Fig. 1(a). The broad absorption band centered at $\sim$3200 cm^{-1} is fitted with three Lorentz terms labeled $L2$–$L4$. The optical conductivity above 9000 cm^{-1} is described by two Lorentzians ($L5$ and $L6$) together with a broad, high-energy background ($L7$) due to higher-energy excitations, which is present for all pressures and will not be discussed in the following.

The profile of the optical conductivity of ZrSiTe at ambient/low pressure is distinctly different from that of other ZrXY materials, whose optical conductivity has a characteristic U shape [19,25]. As an example, we include in Fig. 1(b) the σ_1 spectrum of ZrSiS at ambient pressure. The low-energy range (<6000 cm^{-1}) of the U-shaped optical conductivity stems from transitions between linearly crossing bands along a surface in the Brillouin zone, forming an effective nodal plane [19]. In contrast, the optical conductivity of ZrSiTe does not show a U shape, but the low-energy region is dominated by a broad absorption band at $\sim$3200 cm^{-1} ($\sim$0.4 eV), which we attribute to transitions between electronic bands close to E_F. According to theoretical calculations, the near-E_F electronic band structure of ZrSiTe contains the linearly dispersing bands of the nodal line, like in ZrSiS, but with a larger energy gap due to the larger spin-orbit coupling (energy gap size $\sim$60 meV in ZrSiTe as compared to $\sim$20 meV in ZrSiS) [9,15,17,20]. Additionally, in ZrSiTe nonsymmorphic band crossings appear close to E_F, with an energy separation $\Delta E_{bc} \approx 0.4$ eV at the X point of the Brillouin zone [15]. These band crossings also contribute to the low-energy interband transitions in ZrSiTe [19], though it is difficult to relate them to one specific contribution ($L2$–$L4$) of the broad absorption band.

With increasing pressure, the optical response of ZrSiTe changes drastically over the whole studied energy range (see Fig. 1 and the Supplemental Material [22]). For pressures up to $P_{c1} \approx 4.1$ GPa the overall reflectivity decreases and the plateau in the frequency range 2500–7000 cm^{-1} disappears. The two Drude terms in the low-energy optical conductivity lose spectral weight and sharpen. Most interestingly, the absorption band at $\sim$3200 cm^{-1} undergoes major pressure-induced changes: Its contributions $L2$ and $L3$ shift to lower energies, whereas its high-energy shoulder (contribution $L4$) shifts to higher energies [see Fig. 2(c)]. The $L4$ term might be related to transitions involving the nonsymmorphic band crossings, since these are expected to shift away from E_F with

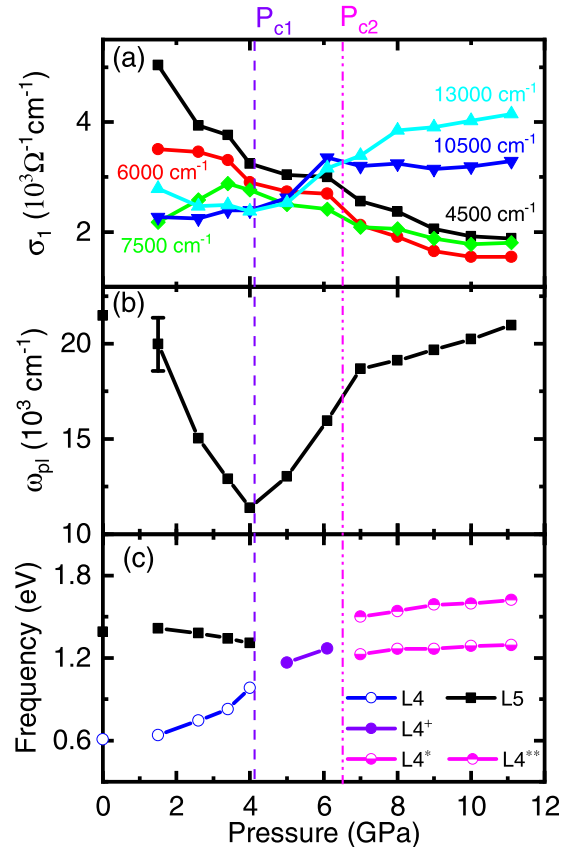

FIG. 2. Pressure dependence of (a) σ_1 at various frequencies and (b) plasma frequency ω_{pl} obtained from the spectral weight of the Drude terms $D1$ and $D2$. (c) Pressure-dependent frequency positions of the contributions $L4$ and $L5$ below P_{c1} and their evolution at higher pressures ($L4^\dagger$, $L4^*$, $L4^{**}$; see text for more details). The dashed and dashed-dotted vertical lines mark the pressures P_{c1} and P_{c2}, respectively.

increasing pressure (decreasing c/a ratio), with a concomitant increase in ΔE_{bc} [15]. Besides, the contributions $L3$ and $L4$ broaden and $L2$ sharpens under pressure, whereas the term $L5$ slightly shifts to lower energies, loses spectral weight, and disappears at P_{c1} [see Fig. 2(c) and Supplemental Material [22] for more details].

For pressures between P_{c1} and 6.1 GPa the low-energy ($\leqslant$5000 cm^{-1}) reflectivity increases with increasing pressure [see Fig. 1(a)], signalling an increasing metallic character. The low-energy profile of σ_1 is dominated by a rather sharp $L2$ peak and a broad $L3$ contribution, besides the two Drude terms $D1$ and $D2$, whose spectral weight shows a pressure-induced increase as revealed by the increasing ω_{pl} [Fig. 2(b)]. At around 10 000 cm^{-1} a contribution $L4^\dagger$ appears, and $L6$ shifts into the measured frequency range. For illustration, we show in Fig. 1(f) the optical conductivity spectrum at 6.1 GPa together with the contributions obtained from the Drude-Lorentz fitting.

At $P_{c2} \approx 6.5$ GPa a splitting of the $L4^\dagger$ peak into two terms $L4^*$ and $L4^{**}$ occurs. Above P_{c2} the increase of the low-frequency reflectivity continues. A more well-defined plasma edge forms [see Fig. 1(a)], which is manifested in the loss function by a plasmon mode, located at $\sim$6700 cm^{-1}

for 11.1 GPa [see Fig. 1(c)]. The profile of the optical conductivity at high pressures is markedly different from the low-pressure regimes [see Fig. 1(g)]: The low-energy range is dominated by two Drude terms and the two sharp low-energy Lorentzians $L1$ and $L2$, followed by a broad and less pronounced excitation $L3$. The higher-energy ($\geqslant 7000$ cm^{-1}) optical conductivity contains the two Lorentz terms $L4^{*}$ and $L4^{**}$, which slightly shift to higher energies and gain spectral weight with increasing pressure, and the term $L6$.

The abrupt pressure-induced changes in the optical response of ZrSiTe at $P_{c1} \approx 4.1$ GPa and $P_{c2} \approx 6.5$ GPa are manifested by anomalies in the pressure dependence of several optical parameters, namely in (i) the screened plasma frequency ω_{pl}^{scr} [Fig. 1(d)], (ii) σ_1 at various frequencies [Fig. 2(a)], and (iii) the plasma frequency ω_{pl} as obtained from the spectral weight of the Drude terms $D1$ and $D2$ [Fig. 2(b)]. These anomalies suggest the occurrence of phase transitions—either structural or electronic—at the critical pressures P_{c1} and P_{c2}. Apparently, both intraband and interband transitions abruptly change at P_{c1} and P_{c2}, suggesting that the phase transitions strongly affect the electronic band structure for energies -1 eV $\leqslant E_F \leqslant 1$ eV and thereby the FS.

Overall, the observed drastic changes in the optical properties show that the electronic band structure of ZrSiTe is highly sensitive to external pressure, whereby ZrSiTe remains metallic at all studied pressures. Our results indicate that pressure pushes some electronic bands towards the Fermi level, whereas others are shifted away from E_F, with effects on both the intraband as well as the interband transitions. The former is manifested by strong changes in ω_{pl}, whereas the latter by (i) additional contributions to $\epsilon_1(\omega)$ in the higher-energy range (above $\sim$7000 cm^{-1}), shifting the zero crossing of $\epsilon_1(\omega)$ to lower energies concomitant with a decrease in ω_{pl}^{scr} over the whole studied pressure range, in contrast to the behavior of ω_{pl}, and (ii) redistribution of spectral weight over the whole energy range (see also Fig. S3 in the Supplemental Material [22]). It is important to note that for all pressures, the profile of the optical conductivity of ZrSiTe does not resemble that of ZrSiS [see Fig. 1(b)]. In particular, the U shape of the optical conductivity, which is characteristic for several ZrXY compounds [19], is not observed for ZrSiTe at any pressure. Accordingly, pressurized ZrSiTe seems to be quite different from ambient-pressure ZrSiS regarding its electronic band structure, although a significant decrease of the c/a ratio of ZrSiTe under pressure is to be expected.

We furthermore note that for ZrSiS, with a much reduced c/a ratio at ambient conditions, the occurrence of a pressure-induced topological quantum phase transition for rather low pressures between 0.16 and 0.5 GPa was recently proposed based on Shubnikov–de Haas measurements [26]. In another topological material with a layered crystal structure, $ZrTe_5$, the variation of the interlayer interaction was suggested as a possible reason for the observed topological phase transition induced by temperature [27,28]. For a detailed interpretation of the pressure-dependent optical response, information on the crystal structure and electronic band structure of ZrSiTe under pressure is needed.

In conclusion, the strong effects of external pressure on the optical response functions (reflectivity, optical conductivity, loss function) in the whole studied frequency range show that the electronic band structure of ZrSiTe is highly sensitive to pressures. Our observations of the pressure dependence of the plasma frequency optical conductivity indicate that under pressure some electronic bands are pushed towards E_F, whereas others shift away from E_F, affecting both intraband and interband transitions. Several optical parameters show anomalies in their pressure dependence at $P_{c1} \approx 4.1$ GPa and $P_{c2} \approx 6.5$ GPa, suggesting the occurrence of two phase transitions of either structural or electronic type.

C.A.K. acknowledges financial support from the Deutsche Forschungsgemeinschaft (DFG), Germany, through Grant No. KU 1432/13-1. The sample synthesis and characterization efforts were supported by the U.S. Department of Energy under Grant No. DE-SC0019068.

[1] A. A. Burkov, M. D. Hook, and L. Balents, Phys. Rev. B **84**, 235126 (2011).
[2] M. Neupane, S. Xu, R. Sankar, N. Alidoust, G. Bian, C. Liu, I. Belopolski, T.-R. Chang, H.-T. Jeng, H. Lin, A. Bansil, F. Chou, and M. Z. Hasan, Nat. Commun. **5**, 3786 (2014).
[3] C. Fang, Y. Chen, H.-Y. Kee, and L. Fu, Phys. Rev. B **92**, 081201(R) (2015).
[4] Y.-Y. Lv, B.-B. Zhang, X. Li, S.-H. Yao, Y. B. Chen, J. Zhou, S.-T. Zhang, M.-H. Lu, and Y.-F. Chen, Appl. Phys. Lett. **108**, 244101 (2016).
[5] R. Sankar, G. Peramaiyan, I. P. Muthuselvam, C. J. Butler, K. Dimitri, M. Neupane, G. N. Rao, M.-T. Lin, and F. C. Chou, Sci. Rep. **7**, 40603 (2017).
[6] J. Hu, Z. Tang, J. Liu, Y. Zhu, J. Wei, and Z. Mao, Phys. Rev. B **96**, 045127 (2017).
[7] N. P. Armitage, E. J. Mele, and A. Vishwanath, Rev. Mod. Phys. **90**, 015001 (2018).
[8] Q. Xu, Z. Song, S. Nie, H. Weng, Z. Fang, and X. Dai, Phys. Rev. B **92**, 205310 (2015).
[9] L. M. Schoop, M. N. Ali, C. Strasser, A. Topp, A. Varykhalov, D. Marchenko, V. Duppel, S. S. P. Parkin, B. V. Lotsch, and C. R. Ast, Nat. Commun. **7**, 11696 (2016).
[10] S. Klemenz, S. Lei, and L. M. Schoop, arXiv:1808.06619.
[11] C. Wang and T. Hughbanks, Inorg. Chem. **34**, 5524 (1995).
[12] M. N. Ali, L. M. Schoop, C. Garg, J. M. Lippmann, E. Lara, B. Lotsch, and S. S. P. Parkin, Sci. Adv. **2**, e1601742 (2016).
[13] R. Singha, A. K. Pariari, B. Satpati, and P. Mandal, Proc. Natl. Acad. Sci. USA **114**, 2468 (2017).
[14] H. A. Klein Haneveld and F. Jellinek, Rec. Trav. Chim. Pays-Bas **83**, 776 (1964).
[15] A. Topp, J. M. Lippmann, A. Varykhalov, V. Duppel, B. V. Lotsch, C. R. Ast, and L. M. Schoop, New J. Phys. **18**, 125014 (2016).
[16] J. Hu, Z. Tang, J. Liu, X. Liu, Y. Zhu, D. Graf, K. Myhro, S. Tran, C. N. Lau, J. Wei, and Z. Mao, Phys. Rev. Lett. **117**, 016602 (2016).
[17] M. Neupane, I. Belopolski, M. M. Hosen, D. S. Sanchez, R. Sankar, M. Szlawska, S.-Y. Xu, K. Dimitri, N. Dhakal,

P. Maldonado, P. M. Oppeneer, D. Kaczorowski, F. Chou, M. Z. Hasan, and T. Durakiewicz, Phys. Rev. B **93**, 201104(R) (2016).

[18] S. M. Young and C. L. Kane, Phys. Rev. Lett. **115**, 126803 (2015).

[19] J. Ebad-Allah, J. F. Afonso, M. Krottenmüller, J. Hu, Y. L. Zhu, Z. Q. Mao, J. Kuneš, and C. A. Kuntscher, Phys. Rev. B **99**, 125154 (2019).

[20] M. M. Hosen, K. Dimitri, I. Belopolski, P. Maldonado, R. Sankar, N. Dhakal, G. Dhakal, T. Cole, P. M. Oppeneer, D. Kaczorowski, F. Chou, M. Z. Hasan, T. Durakiewicz, and M. Neupane, Phys. Rev. B **95**, 161101(R) (2017).

[21] R. Singha, S. Samanta, S. Chatterjee, A. Pariari, D. Majumdar, B. Satpati, L. Wang, A. Singha, and P. Mandal, Phys Rev. B **97**, 094112 (2018).

[22] See Supplemental Material at http://link.aps.org/supplemental/10.1103/PhysRevB.99.245133 for details about sample preparation, experimental details, additional experimental results, and analysis of the pressure-dependent optical conductivity spectra.

[23] R. Wooten, *Optical Properties of Solids* (Academic Press, New York, 1972).

[24] The lowest-energy Lorentz term $L1$ strongly overlaps with the Drude terms $D1$ and $D2$, and is therefore hard to distinguish. Taking into account the spectral weight of $L1$ in the sum rule according to $\omega_{pl}^2/8 = \int_0^\infty [\sigma_{1,D1}(\omega) + \sigma_{1,D2}(\omega) + \sigma_{1,L1}(\omega)]d\omega$ gives the plasma frequency $\omega_{pl} = 24\,730\ \mathrm{cm}^{-1}$. It is important to note that the anomalies in ω_{pl} as a function of pressure are observed independent of whether or not the spectral weight of the Lorentz term $L1$ is taken into account in the sum rule.

[25] M. B. Schilling, L. M. Schoop, B. V. Lotsch, M. Dressel, and A. V. Pronin, Phys. Rev. Lett. **119**, 187401 (2017).

[26] D. VanGennep, T. A. Paul, C. W. Yerger, S. T. Weir, Y. K. Vohra, and J. J. Hamlin, Phys. Rev. B **99**, 085204 (2019).

[27] Y. Zhang, C. Wang, L. Yu, G. Liu, A. Liang, J. Huang, S. Nie, X. Sun, Y. Zhang, B. Shen, H. Liu, U. Weng, L. Zhao, G. Chen, X. Jia, C. Hu, Y. Ding, W. Zhao, Q. Gao, C. Li *et al.*, Nat. Commun. **8**, 15512 (2017).

[28] B. Xu, L. X. Zhao, P. Marsik, E. Sheveleva, F. Lyzwa, Y. M. Dai, G. F. Chen, X. G. Qiu, and C. Bernhard, Phys. Rev. Lett. **121**, 187401 (2018).